

SIMULATION OF CRACK PROPAGATION IN RC SHEAR WALL USING A 3D RIGID-BODY-SPRING MODEL WITH RANDOM GEOMETRY

YOSHIHITO YAMAMOTO*, HIKARU NAKAMURA, ICHIRO KURODA* AND
NOBUAKI FURUYA***

* National Defense Academy of Japan
Department of Civil and Environmental Engineering, Yokosuka, Japan
e-mail: yyama@nda.ac.jp, www.mod.go.jp/nda/

** Nagoya University
Department of Civil Engineering, Nagoya, Japan
e-mail: hikaru@nagoya-u.jp, www.civil.nagoya-u.ac.jp

Key words: Discrete modeling, Rigid-Body-Spring model, Crack propagation, Shear wall, Cyclic loading

Abstract: The use of a discrete-type numerical approach based on the three-dimensional Rigid-Body-Spring Model (RBSM) is proposed to simulate the crack propagation behavior of reinforced concrete (RC) shear walls subjected to monotonic and cyclic loadings, which are tested in the context of the international benchmark ConCrack (<http://www.concrack.org/>). In the RBSM, concrete is modeled as an assemblage of rigid particles interconnected by springs along their boundaries. The proposed model in this study utilizes the random particle configuration obtained from Voronoi tessellation, which reduces mesh bias on potential cracking directions. Reinforcing bar is modeled by a series of beam elements and load transfer between the beam nodes and the concrete particles is provided by linkage elements. The bond-slip characteristic of the reinforcing bar is introduced to the linkage spring. This model can realistically simulate localized and oriented phenomena, such as cracking, its propagation, frictional slip and so on, in concrete structures. The authors have already developed the constitutive models for the above mentioned model and the model has been validated through the simulations of the responses of concrete specimen subjected to uniaxial tension, uniaxial and triaxial compression. It can simulate not only tensile cracking but also fracture localization in compression. In this study, the constitutive models were extended to include cyclic effects and the model was validated through the simulations of the RC panel tests under cyclic loadings, which were reported in the literatures. Furthermore, the simulations of the RC shear wall tests were carried out, and the capability of the model to predict the detailed cracking information, such as crack width, spacing and direction of propagation is discussed.

1 INTRODUCTION

Recent years, the development of accurate and reliable estimation method of the detailed cracking information in reinforced concrete (RC) structures, such as the crack width and crack spacing, is desired in the view point of maintenance and long-life of buildings.

Cracks originate and propagate by various

actions, e.g. applied load, shrinkage, thermal expansion, corrosion of steel reinforcement. Moreover, the crack propagation behaviors are strongly affected by the dimension and shape of member, boundary condition, arrangement of reinforcement. Numerical methods such as nonlinear finite element method are the effective tools for the predictions of the

cracking behavior, which simultaneously take into account the various actions and conditions as described above. However, the study focused on the applicability of numerical methods for the crack propagation behaviors in RC member is limited and the validation of applicability is not sufficient.

There are two prominent types of numerical methods for concrete structures, which are continuum methods and discrete-type numerical methods. Discrete-type numerical methods have advantages in modeling localized and oriented phenomena, such as cracking, its propagation, frictional slip and so on, in RC structures, relative to smeared-crack continuum models.

The Rigid-Body-Spring Model (RBSM) developed by Kawai [1] is one of the discrete-type methods. Bolander and Saito [2] introduced a random geometry to the RBSM mesh using Voronoi tessellation and have shown that the model can simulate the crack patterns, the deformation and the load capacity of concrete materials and RC structures successfully. Suzuki et al. [3] and Nagai et al. [4] have carried out simulations of concrete material by the three-dimensional (3D) RBSM, and have shown that the model can represent the multi-axial compression and localization behaviors with the simple constitutive models. These previous studies indicate that the RBSM is the promising numerical method for the concrete structures.

In this study, the use of the 3D RBSM is proposed to simulate the crack propagation behavior of RC shear walls subjected to monotonic and cyclic loadings, which were tested in the context of the national French

project “CEOS.fr” (<http://www.concrack.org/>). The tests aim to create the benchmark for the current cracking assessment method.

The authors have already developed constitutive models for the 3D RBSM [5] in order to quantitatively evaluate the mechanical responses including softening and localization fractures, and have shown that the model can well simulate the cracking and failure behaviors of RC beams [6,7]. In this study, the constitutive models are extended to include cyclic effects and the model was validated through the simulations of the RC panel tests under cyclic loadings, which were reported in the literatures. Next, the simulations of the RC shear wall tests mentioned above were carried out, and the capability of the model to predict the detailed cracking information, such as crack width, spacing and direction of propagation is discussed.

2 NUMERICAL MODELS

2.1 RBSM

In RBSM, concrete is modeled as an assemblage of rigid particles interconnected by springs along their boundary surfaces (Figure 1a). The crack pattern is strongly affected by the mesh design as the cracks initiate and propagate through the interface boundaries of particles. Therefore, a random geometry of rigid particles is generated by a Voronoi diagram (Figure 1b), which reduces mesh bias on the initiation and propagation of potential cracks.

The response of the spring model provides an insight into the interaction among the particles, which is different from models based

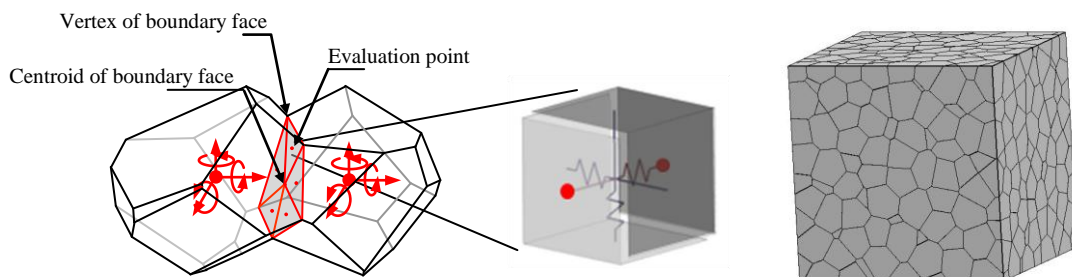


Figure 1: (a) Rigid-body-spring model and (b) Voronoi diagram

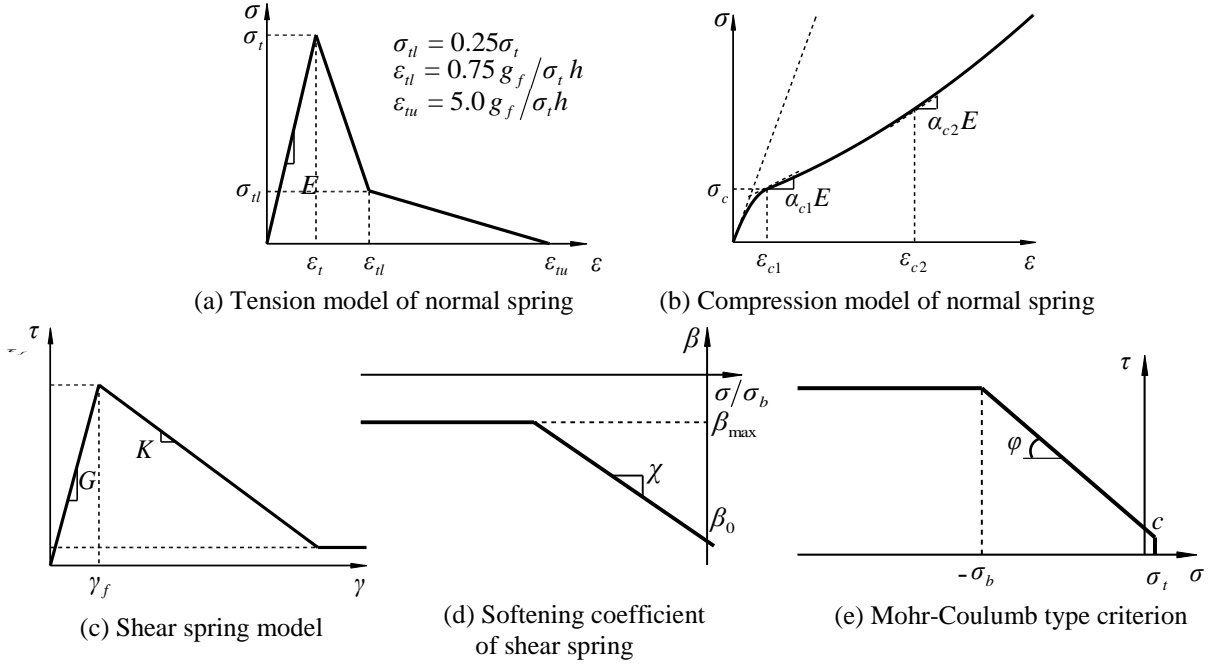


Figure 2: Constitutive model for concrete [5]

on continuum mechanics. In this model, each rigid particle has three translational and three rotational degrees of freedom defined at the nuclei (or nodal points) that define the particles according to the Voronoi diagram (Figure 1a). The boundary surface of two particles is divided into several triangles with a center of gravity and vertices of the surface as seen in the figure. One normal and two shear springs are set at the center of each triangle. By distributing the springs in this way, over the Voronoi facet common to two neighboring nodal points, this model accounts for the effects of bending and torsional moment without the need to set any rotational springs [5].

2.2 Modeling of concrete material

The constitutive models for tension, compression and shear that are used in 3D RBSM are shown in Figure 2 [5]. The tensile model for normal springs is shown in Figure 2a. Up to tensile strength, the tensile behavior of concrete is modeled as linear elastic and, after cracking, a bilinear softening branch according to a 1/4 model is assumed. In the model, σ_t , g_f and h represent tensile strength, tensile fracture energy, and distance between

nuclei, respectively. The model takes into consideration tensile fracture energy.

Figure 2b shows the stress–strain relation for compression of normal springs that was modeled as an S-shape curve combining two quadratic functions [5]. The parameters of σ_c , ε_{c1} and α_{c1} and α_{c2} shown in Figure 2b are material parameters which controlled the nonlinearity of the compression behavior of the normal spring.

The shear stress–strain relation represents the combination of two shear springs. The combined shear strain is defined by Eq. (1), in which γ_l and γ_m represent the strains of the springs in each direction shear to the fracture surface. Then, combined shear stress τ is calculated from the shear stress–strain relation, and the shear stresses for each direction (τ_l and τ_m) are distributed by Eq. (2).

$$\gamma = \sqrt{\gamma_l^2 + \gamma_m^2} \quad (1)$$

$$\tau_l = \tau \frac{\gamma_l}{\gamma}, \quad \tau_m = \tau \frac{\gamma_m}{\gamma} \quad (2)$$

The envelope of the stress–strain relationship for shear is given in Figure 2c, Eq. (3) and Eq. (4). In the model, τ_f , γ_f and γ_{\max}

represent shear strength, strain corresponding to strength and the maximum value of γ in loading history, respectively. The stress elastically increases up to the shear strength with the slope of shear modulus G and softening behavior is also assumed. K is the shear-softening coefficient that is defined by Eq. (4). It is assumed that the shear softening coefficient K depends upon the stress of the normal spring as represented in Eq. (4) and Figure 2d, where, β_0 , β_{\max} and χ are the parameters of dependency on the normal spring for the shear-softening coefficient.

$$\tau = \begin{cases} G\gamma & (\gamma < \tau_{f,soft} / G) \\ \tau_{f,soft} & (\gamma \geq \tau_{f,soft} / G) \end{cases} \quad (3)$$

$$\tau_{f,soft} = \max(\tau_f + K\langle \gamma_{\max} - \gamma_f \rangle, 0.1\tau_f) \quad (4a)$$

$$K = \beta G \quad (4b)$$

$$\beta = \min(\beta_0 + \chi(\sigma / \sigma_b), \beta_{\max}) \quad (4c)$$

where the brackets $\langle \cdot \rangle$ in Eq.(4a) is defined as $\langle x \rangle = \max(x, 0)$. The Mohr–Coulomb criterion is assumed as the failure criteria for the shear spring (Figure 2e and Eq.(5)), where c and φ are cohesion and the angle of internal friction, respectively. The shear strength is assumed to

be constant when the normal stress is greater than σ_b , which is termed the compression limit value.

$$\tau_f = \begin{cases} c - \sigma \tan \varphi & (\sigma > -\sigma_b) \\ c + \sigma_b \tan \varphi & (\sigma \leq -\sigma_b) \end{cases} \quad (5)$$

Moreover, it is assumed that the shear stress decreases with an increase in crack width at the cracked surface, in which tensile softening occurs in a normal spring by taken into consideration the shear deterioration coefficient β_{cr} as represented in Eq. (6), which is similar to Saito's model [8]. Here, ε_t and ε_{tu} are cracking strain and ultimate strain in a normal spring, respectively.

$$\beta_{cr} = \frac{\varepsilon_t}{\varepsilon} \exp\left\{\frac{\kappa}{\varepsilon_{tu}}(\varepsilon - \varepsilon_t)\right\} \quad (6)$$

The material parameters of the constitutive models as described above has been calibrated by conducting parametric analyses comparing with the test results of uniaxial tension, uniaxial compression, hydrostatic compression and triaxial compression. The parametric analyses include a variety of specimen size, shape, mesh size and concrete strengths. The calibrated parameters are shown in Table 1.

Table 1. Model parameters [5]

Normal spring							Shear spring							
Elastic modulus	Tensile response		Compressive response				Elastic modulus	Fracture criterion			Softening behavior			
E N/mm ²	σ_t N/mm ²	g_f N/mm ²	σ_c N/mm ²	ε_{c2}	α_{c1}	α_{c2}	$\eta=G/E$	c N/mm ²	φ degree	σ_b N/mm ²	β_0	β_{\max}	χ	κ
$1.4E^*$	$0.8f_t^*$	$0.5G_f^*$	$1.5f_c'^*$	-0.015	0.15	0.25	0.35	$0.14f_c'^*$	37	$f_c'^*$	-0.05	-0.02	-0.01	-0.3

* The macroscopic material parameters obtained from the concrete specimens tests

E^* : Young's modulus, f_t^* : Tensile strength, G_f^* : Fracture energy, $f_c'^*$: Compressive strength

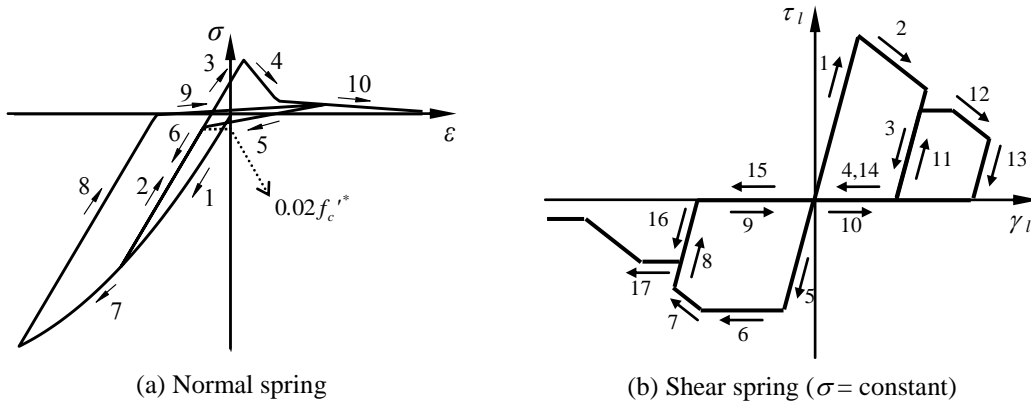


Figure 3: Hysteresis of stress – strain relation

These parameters are recommended for normal strength concrete. Moreover, the average size of the Voronoi particles (mesh size) to use the parameters was recommended from 10 mm to 30 mm [5].

The compression model considers neither softening behavior nor failure of the normal springs. However, compressive failure behavior can be simulated with a confinement effect by means of a combination of a normal spring and a shear spring.

Figure 3a shows the typical hysteresis loop of the normal spring under reversed cyclic loading, which is newly introduced to the previously proposed model described above. The unloading paths in the tension zone pass toward the point of stress $\sigma = -0.02f'_c$ on the compression loading path. The reloading paths in the tension zone pass toward the start point of the unloading. The stiffness of the unloading in the compression zone is initial elastic modulus E .

Figure 3b shows the typical hysteresis loop of the shear spring. The stiffness of the unloading and reloading is initial elastic modulus G . In addition, after the stress reaches zero on the unloading path, the stress keeps zero until the strain reaches the residual strain of the opposite sign.

2.3 Modeling of reinforcing bar and bond interface

Reinforcement is modeled as a series of regular beam elements (Figure 4) that can be freely located within the structure, regardless of the concrete mesh design [2]. Three translational and three rotational degrees of freedom are defined at each beam node. The reinforcement is attached to the concrete particles by means of zero-size link elements that provide a load-transfer mechanism between the beam node and the concrete particles. For the reinforcing bar, the bilinear kinematic hardening model is applied. The hardening coefficient is 1/100. Crack development is strongly affected by the bond interaction between concrete and reinforcement. The bond stress–slip relation is provided in the spring parallel to the

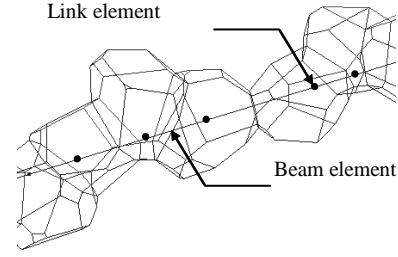


Figure 4: Reinforcement models

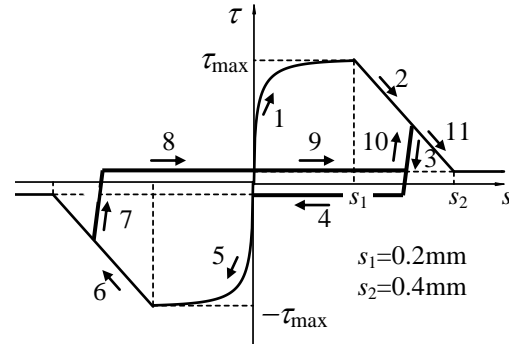


Figure 5: Bond - slip relation

reinforcement of linked element. Figure 5 shows the relation that is defined by Eq. (7) up to peak strength [9], and the curve proposed by CEB-FIB is assumed after peak strength [10].

$$\tau = 0.36(f'_c)^{2/3} \left[1 - \exp\left\{-40(s/D)^{1/2}\right\} \right] \quad (7)$$

where D is the diameter of the reinforcement and s represents slippage.

3 SIMULATION OF RC PANEL UNDER CYCLIC LOAD

3.1 Test overview and numerical model

In order to validate the applicability of the proposed model for cyclic shear responses, the tests of RC panels under reversed cyclic in-plane shear stress, which were conducted by Omori et al. [11], are simulated. Figure 6 shows the geometry of a typical specimen. The panels were loaded in pure shear, with shear force applied via shear keys around the perimeter of the specimen. The principal test parameter is reinforcement ratio, as shown in Table 2. The reinforcement ratios in both directions are the same. Figure 7 shows the numerical model of RC panel. Considering the computational costs of simulations of the cyclic loadings, the average size of the

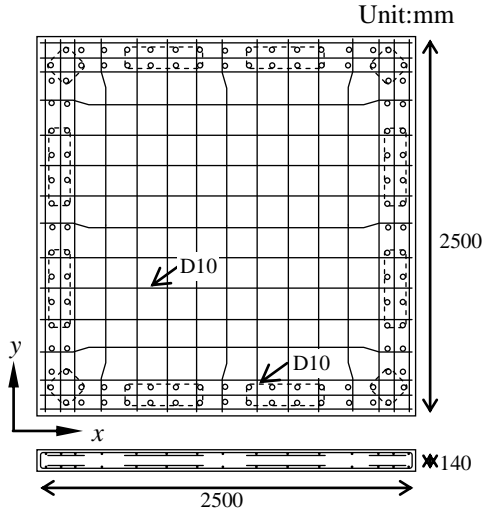


Figure 6: Typical test specimen (SR05)

Table.2 Test Parameter and material properties

Specimen	SR05	SR10	SR14	SR17	SR20
Concrete					
Compression strength, MPa	30.4	36.6	29.3	28.7	31.2
Reinforcement					
Bar type	D10				
Bar area, mm ²	71.3				
Yield strength, MPa	398				
Reinforcing ratio ($\rho_x = \rho_y$), %	0.51	1.02	1.36	1.70	2.04
Spacing, mm	200	100	75	60	50

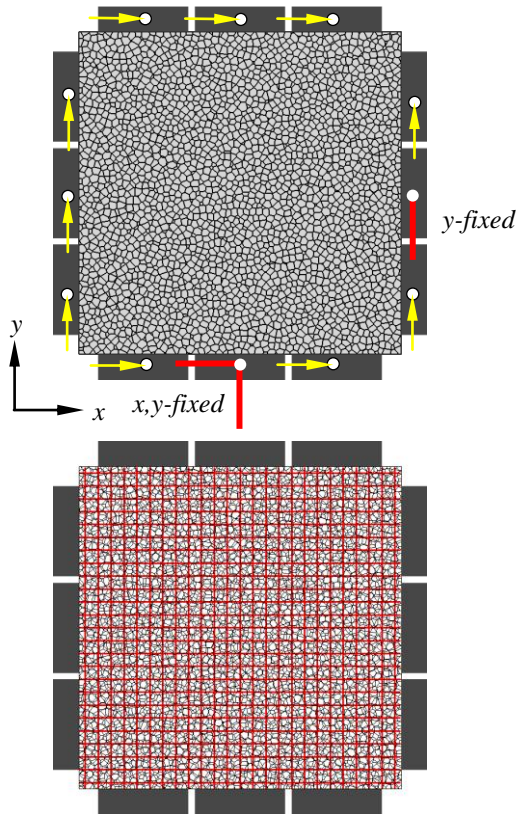


Figure 7: Numerical model (SR10)

particles in the model is approximately 50mm, which is a larger than that used in the calibration analysis [5] as mentioned above. In general for the discrete type modeling, particle size influences the numerical results. However, we confirmed that the average shear stress-strain curves of the RC panels, obtained from the numerical simulations, are not influenced by such difference of the particle size only in the pre-peak regions, while it may be influenced in the post-peak region. Therefore, in this section, the research focuses on the responses in the pre-peak region.

3.2 Comparison of numerical and experimental results

The average shear stress-strain responses obtained from the numerical results are compared with the experimental ones as shown in Figure 8. The numerical predictions agree reasonably with the experimental results.

Figure 9 shows the simulated crack pattern at the point A and B in Figure 8. Figure 10 shows the experimental observation. The crack width shown in Figure 9 means the normal component of the relative displacement between two adjacent particles. It is found that the cracks of numerical predictions propagate through the intersection points of the reinforcing bars as shown in Figure 9(a) and Figure 9(b). It was reported in the literature [11] that the crack spacing decreased as the spacing of the reinforcing bar decreased. The numerical predictions agree with the experimental observation. However, in the case of SR20 whose reinforcing bars spacing close to the particle size, the numerical cracks are not clearly localized. This means that the particle size must be sufficiently smaller than the spacing of the reinforcing bars in order to adequately estimate the crack spacing for these problems.

4 SIMULATION OF RC SHEAR WALL UNDER MONOTONIC AND CYCLIC LOAD

4.1 Test overview and numerical model

The proposed model is applied to simulate

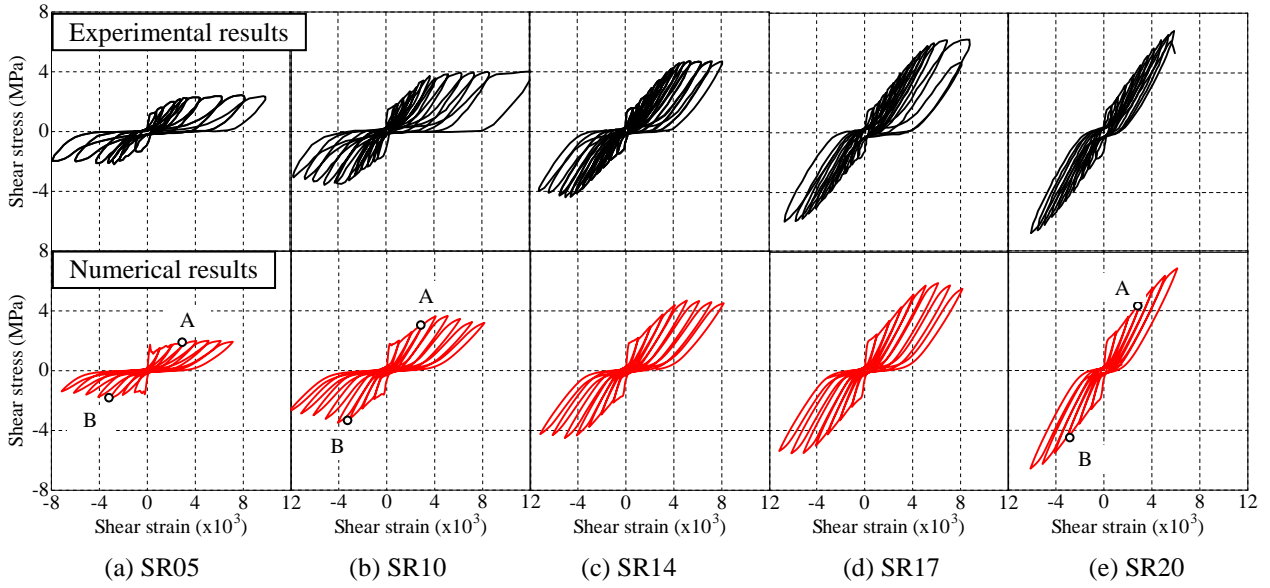


Figure 8: Average shear stress-strain relation

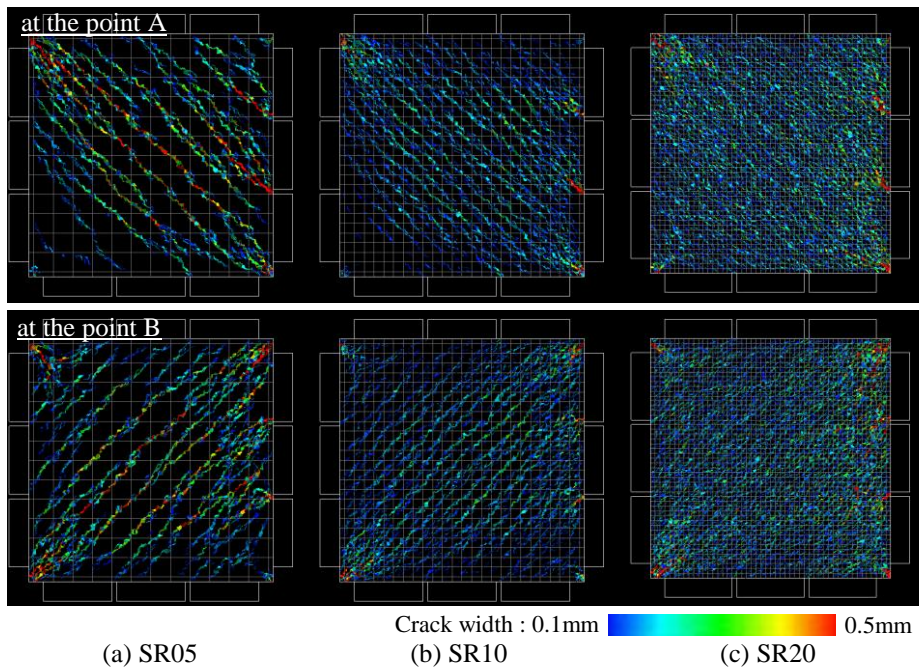


Figure 9: Crack patterns obtained from numerical simulations

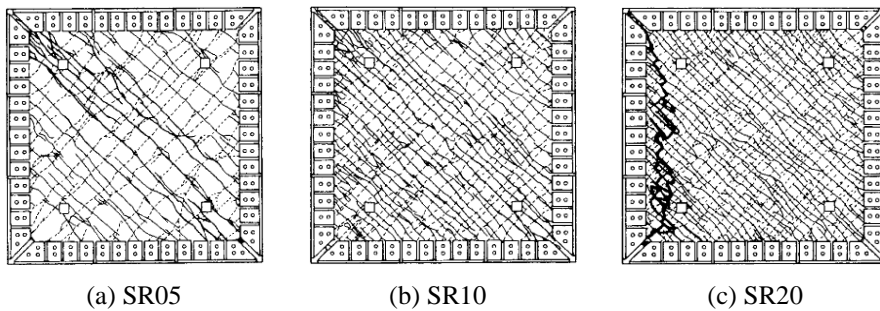


Figure 10: Final crack patterns observed in the experiment [11]

the crack propagation behavior of RC shear walls subjected to monotonic and cyclic loadings, which were tested in the context of the national French project “CEOS.fr” (<http://www.concrack.org/>).

Figure 11 shows the numerical model of the RC shear wall. The color solid lines represent the reinforcing bar. In the testing wall section, the dimensions are 4.20m in length, 1.07m in height and 0.150m in thickness, and the reinforcement ratio is 1% in two layers. Concrete strength used of the test specimens is 42.5MPa. The high strength steel bar of 500MPa grade is used for the reinforcement, and its elastic strain limit is 555MPa. In order to reduce the computational cost, the particle sizes are increased gradually with coming closer to the top and bottom sides of the test specimen. For the testing wall section, the

average particle size set to approximately 40mm.

4.2 Comparison of numerical and experimental results

The load–displacement curves of the experimental and numerical results are compared in Figure 12. For the monotonic loading case, the numerical predictions of the stiffness and the peak load agree well with the experimental results. For the cyclic loading case, the numerical predictions overestimate the displacement at the peak load. However, the shape of the hysteresis loops, the peak load and cyclic degradation of load capacity are well reproduced.

The comparisons of crack patterns in the monotonic loading case at each load step are shown in Figure 13. The white dotted line in

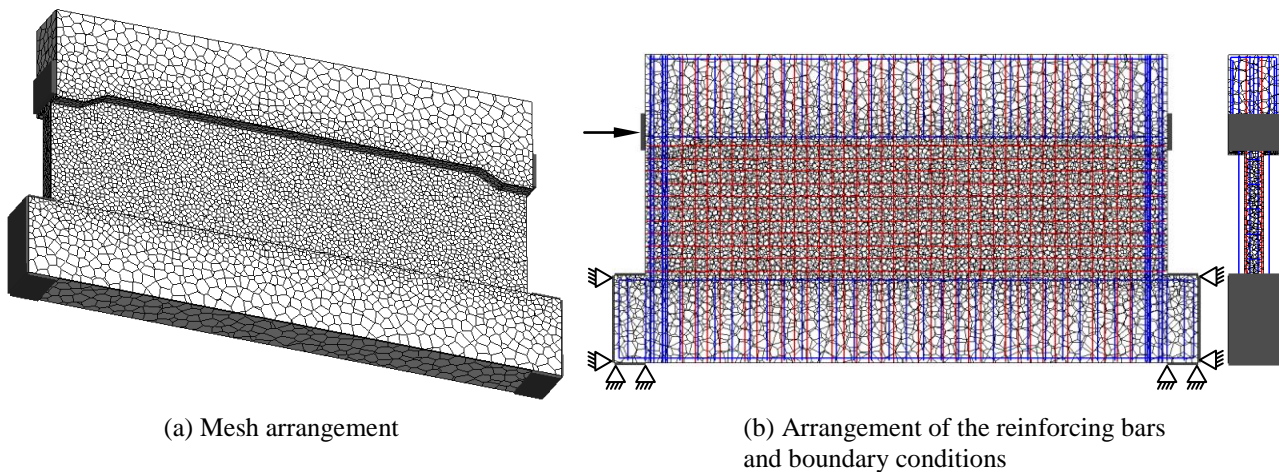


Figure 11: Numerical model

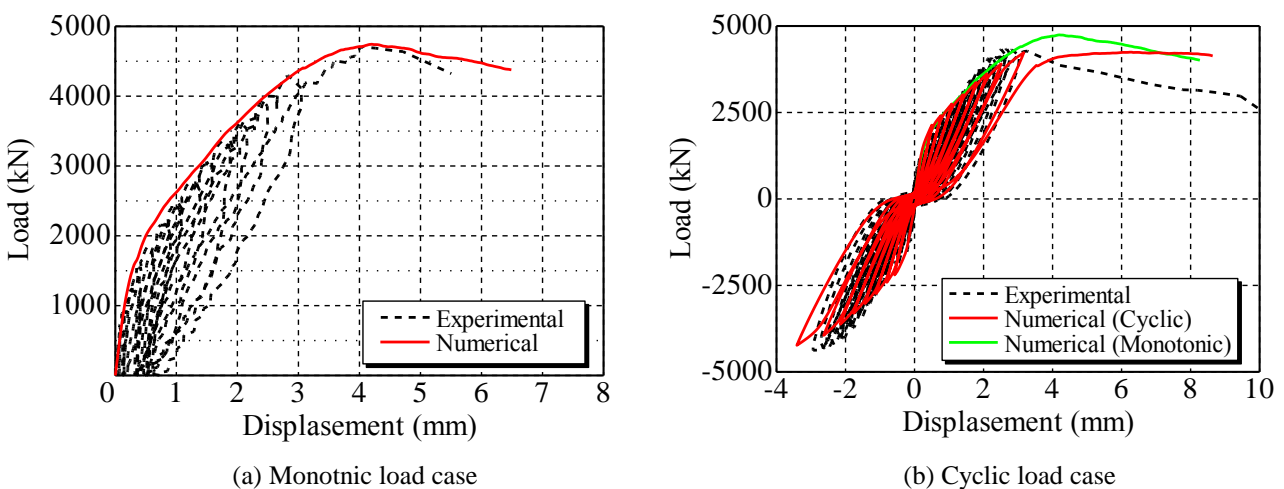
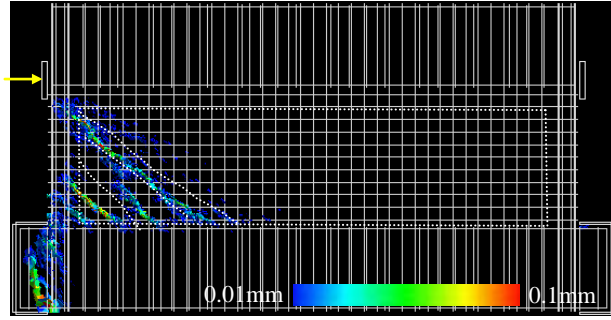
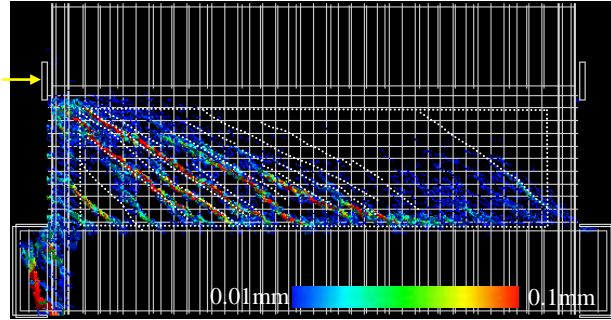


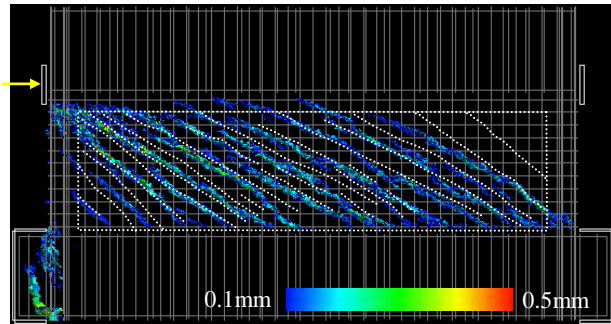
Figure 12: Load and Displacement relation



(a) 1500kN



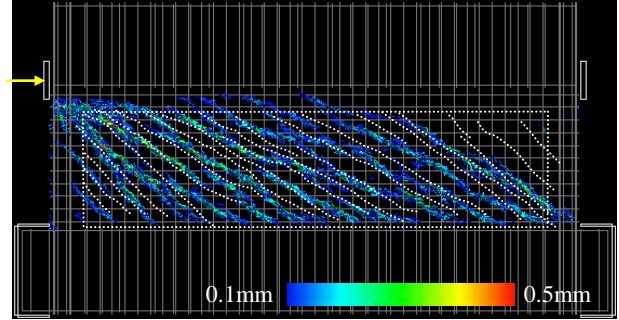
(b) 2700kN



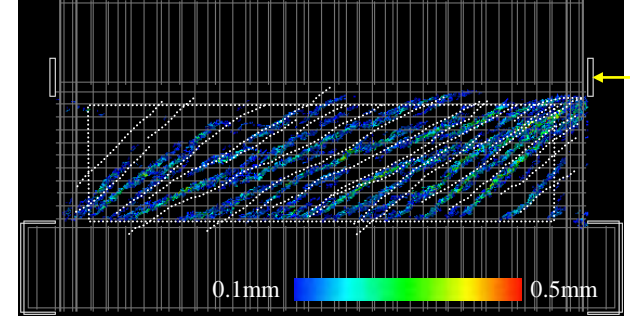
(c) 4200kN

Figure 13: Crack patterns under the monotonic load

Figure 13 show the crack patterns obtained from the experimental observation. The numerical predictions of the crack spacing and the crack angle reasonably agree with the experimental observations. The maximum crack width obtained from the experiment at each step is approximately 0.04mm at the load $P = 1500$ kN, approximately 0.06mm at the load $P = 2700$ kN and approximately 0.34mm at the load $P = 4200$ kN. The numerical predictions tend to overestimate the crack width on the load-increasing process. The reason is that, since the numerical simulations do not reproduce all of the cracking, for instance, at the load $P = 2700$ kN, the numerical prediction do not reproduce the cracking in the center of the test specimen, the



(a) 4200kN



(b) -4200kN

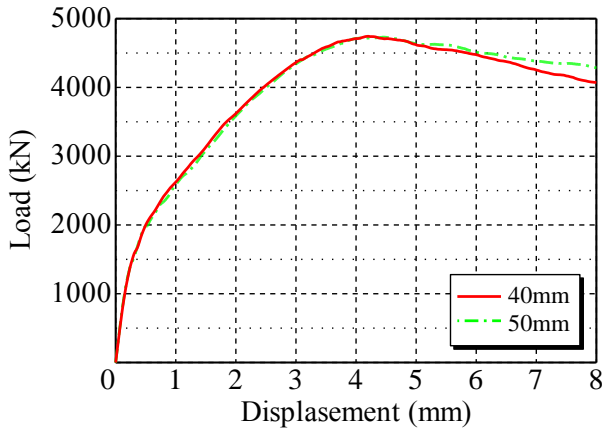
Figure 14: Crack patterns under the cyclic load

extension of the crack width concentrate to the previously occurred cracks. On the other hand, at the load $P = 4200$ kN where the numerical simulations reproduced the majority of all cracks observed in the experiment, the numerical predictions roughly agree with the maximum crack width of experimental results.

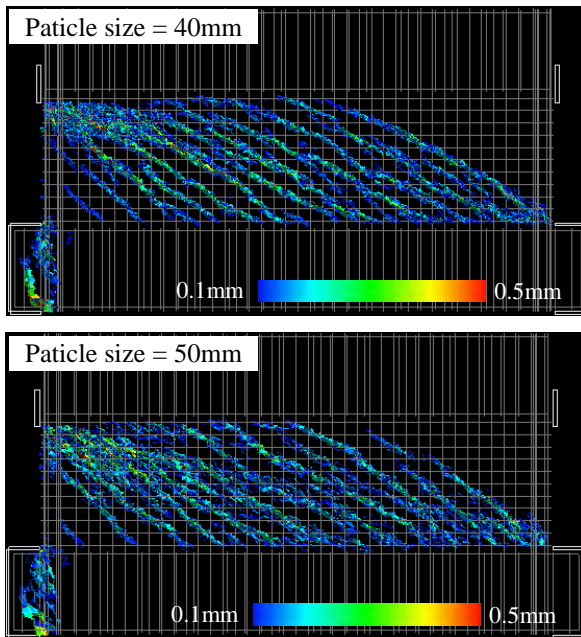
The comparisons of crack patterns in the cyclic loading case at each step are shown in Figure 14. The numerical predictions of the crack spacing and angle reasonably agree with the experimental observation. In addition, the proposed model can simulate the non-orthogonal two-directional cracks as observed in the experiment. The maximum crack widths measured in the experiment is approximately 0.30mm at the load $P = 4200$ kN. The numerical predictions roughly agree with the experimental results.

4.3 Influence of particle size

In order to estimate a dependence of the particle size of the proposed model, an additional numerical simulation under monotonic load, which used the average particle size of approximately 50mm, is conducted. The load–displacement curves of



(a) Load – displacement relation



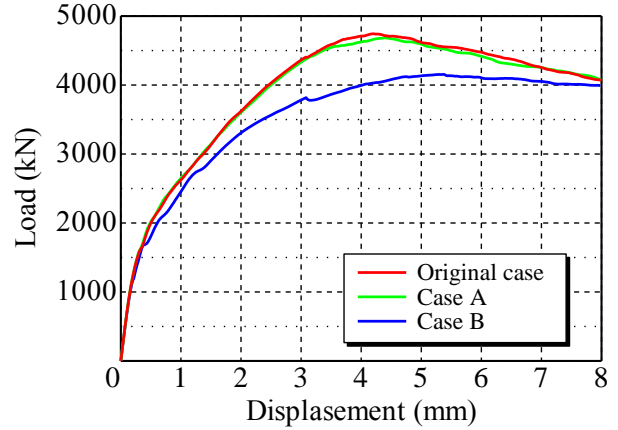
(b) Crack pattern (at the peak load)

Figure 15: Influence of the particle size

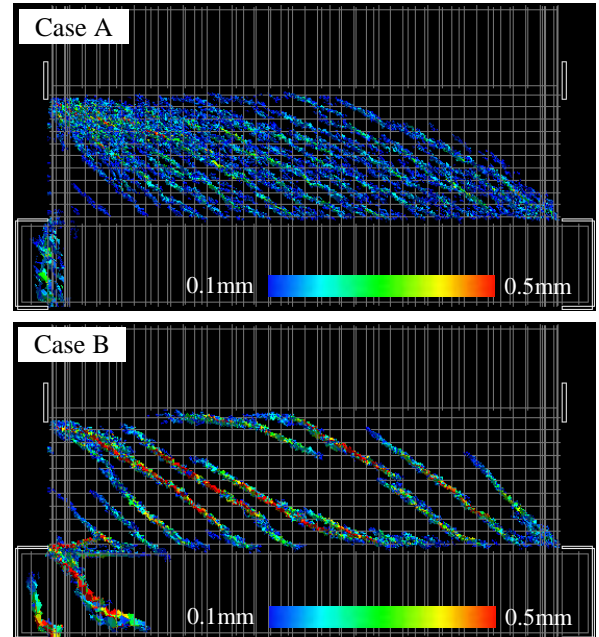
the original case shown above and the additional case are compared in Figure 15a. Nearly the same load-displacement response is obtained with the exception of the post-peak region. The comparisons of crack patterns at the peak-load are shown in Figure 15b. In the case of the larger particle size, definition of the cracks decrease, especially it is observed near the loading point where the crack spacing becomes smaller.

4.4 Influence of bond-slip condition

In order to investigate the influence of bond-slip condition between concrete and reinforcing bars, simulations that changed the



(a) Load – displacement relation



(b) Crack pattern (at the peak load)

Figure 16: Influence of the bond condition

bond strength are conducted.

The load–displacement curves of the original case shown above and the additional cases are compared in Figure 16a. Case A shown in Figure 16 is that the bond strength are changed to twice the value of the original case, and case B is that the bond strength is 1/5 of the original case. The load displacement curves obtained from the original case and case A are nearly same, however, in the case B, the load capacity remarkable decrease.

The comparisons of crack patterns at the peak-load are shown in Figure 16b. In the case A, the crack spacing and the crack width becomes smaller than that of the original case.

On the contrary, in the case B, the crack spacing and the crack width becomes larger than that of the original case. In order to accurately predict the detailed crack information, the model of the bond-slip characteristics is of exceedingly importance.

5 CONCLUSIONS

In this study, the numerical simulations of the RC panels and the RC shear walls under monotonic and cyclic loading were conducted in order to validate the ability of the proposed model which is based on the RBSM to predict the crack propagation behavior, especially paying attention the prediction accuracy of the crack spacing, the crack angle and the crack width.

For the RC panels under cyclic load, the numerical predictions of the average shear stress-strain response and crack patterns reasonably agree well with the experimental observation. However, it is found that the particle size must be sufficiently smaller than the spacing of the reinforcing bars in order to adequately estimate the crack spacing for this problem.

For the RC shear wall under monotonic and cyclic load, the proposed model reasonably predicts not only the load-displacement response but also the crack spacing and the crack angle. Furthermore, the numerical predictions of the crack width at the neighboring point of the peak-load roughly agree with the experimental results. However, on the load-increasing process, the numerical predictions of crack width tend to overestimate the experimental results. The reason is that, since the numerical simulations do not reproduce all of the cracking, the extension of the crack width concentrate to the previously occurred cracks. This discrepancy between numerical and experimental results may be influenced by the initial damage which is caused by shrinkage, thermal deformation and so on.

In addition, the influences of the particle size and the bond-slip condition are estimated. The particle size does not influence the load-displacement response in the pre-peak region.

The post-peak behavior and the damage localization behavior are influenced by the particle size in the range of this study.

The bond strength between concrete and reinforcing bars strongly influence the crack propagation behavior. In order to accurately predict the detailed crack information, the model of the bond-slip characteristics is of exceedingly importance.

REFERENCES

- [1] Kawai, T., 1978. New discrete models and their application to seismic response analysis of structures. *Nuclear Engineering and Design*. **48**:207-229.
- [2] Bolander, J. E., and Saito, S., 1998. Fracture analysis using spring network with random geometry. *Engineering Fracture Mechanics*. **61.5-6**: 569–591.
- [3] Suzuki, T., Saito, S., Higai, T., 2005. Meso-scale analyses of concrete under uniaxial compression. *Proceeding of the Japan Concrete Institute*. **27**:169-174 [In Japanese].
- [4] Nagai, K., Sato, Y., Ueda, T., 2005. Three-dimensional mesoscopic simulation of concrete under biaxial stress condition by RBSM. *Proceeding of the Japan Concrete Institute*. **27**:175-180.
- [5] Yamamoto Y., Nakamura H., Kuroda I., Furuya N., 2008. Analysis of compression failure of concrete by three-dimensional rigid body spring model. *Doboku Gakkai Ronbunshuu E*. **64(4)**:612–630 [in Japanese].
- [6] Gedik Y. H., Nakamura H., Yamamoto Y., and Kunieda M., 2011. Evaluation of Three dimensional Effects in Short Deep Beams using a Rigid Body Spring Model. *Cement and Concrete Composites*. **33-9**:978-991.
- [7] Gedik Y. H., Nakamura H., Yamamoto Y., Ueda N. and Kunieda M., 2012. Effect of

Stirrups on the Shear Failure Mechanism of Deep Beams. *Journal of Advanced Concrete Technology*. **10**:14-30.

- [8] Saito, S., Hikosaka, H., 1999. Numerical analysis of reinforced concrete structures using spring network model. *Journal of Materials, Concrete Structures and Pavements*. **627**:289-303.
- [9] Suga M, Nakamura H, Higai T, Saito S., 2001. Effect of bond properties on the mechanical behavior of RC beam. *Proc Japan Concrete Inst.* **23(3)**:295–300 [in Japanese].
- [10] Comité Euro-International du Béton. 1990. *CEB-FIP Model Code 1990 First Draft*. CEB, Paris.
- [11] Ohmori, N. et al., 1989. Experimental Studies on Nonlinear Behaviours of Reinforced Concrete Panels Subjected to Cyclic In-plane Shear. *Journal of structural and construction engineering. Transactions of AIJ.* **403**:105-118 [in Japanese].